Vision Research 73 (2012) 46–52

Contents lists available at SciVerse ScienceDirect

Vision Research

journal homepage: www.elsevier.com/locate/visres

Increment thresholds for radial frequency trajectories produce a dipper function ☆

Marwan Daar *, Charles C.-F. Or, Hugh R. Wilson

Centre for Vision Research, York University, 4700 Keele Street, Room 0009 CSEB, Toronto, Ontario, Canada M3J 1P3

ARTICLE INFO

Article history:
Received 29 May 2012
Received in revised form 21 August 2012
Available online 3 October 2012

Keywords:
Periodic motion trajectories
Radial frequency motion trajectories
Dipper function

ABSTRACT

Radial frequency (RF) trajectories are a new class of stimuli that have been developed to study the visual perception of periodic motion (Or et al., 2011). These stimuli are described by a moving dot that traces a distorted path through space with periodic radial deformations whose frequency, amplitude, and phase can be independently specified. Here, we extend Or et al.'s findings by investigating how the discrimination of RF amplitude changes as a function of different reference amplitudes in a two-interval forced choice task. Using an RF3 trajectory (a pattern with three cycles of deformation along its trajectory), increment thresholds were measured at six different reference amplitudes: Detection (discriminating a circle from RF3), 1X (discriminating a pair of RF3 patterns, with the amplitude of one member of this pair set to (1X) threshold obtained from the detection condition), 2.5X, 5X, 10X, and 15X. Data show that sensitivity to changes in amplitude improves at 2.5X by a factor of about 2, recovers to detection threshold levels at 5X, and continues to rise at 10X and 15X. These results generalize across both radial frequency and the angular speed of the trajectory, and persist with low contrast trajectories. Our findings point to the existence of a neural mechanism that is sensitive to deviations from circular motion trajectories.

1. Introduction

One of the driving questions in motion perception is how our visual systems integrate information over time and space into an accurate and meaningful representation of our immediate environment (see Burr and Thompson (2011) and Nishida (2011) for a review). A number of methodologies have been employed, showing that we are highly adept at detecting global patterns of motion amidst a noisy background (de la Malla & López-Moliner, 2010), and that we are able to quickly and accurately detect and describe complex patterns of biological motion from impoverished stimuli (Johansson, 1973). Generally, the stimuli in these experiments comprise a field of moving dots, each with its own trajectory, making them powerful tools for understanding perceptual cases such as optic flow and biological motion. Periodic motion trajectories are a novel class of stimuli that have recently been introduced (Or et al., 2011), and allow the study of the perception of isolated motion trajectories. These trajectories, known as radial frequency motion trajectories or RF trajectories, are described by a dot that moves in a periodic path in polar coordinates whose radius undergoes a sinusoidal modulation. They are a potentially fruitful class of stimulus to explore for several reasons. First, they are biologically relevant. Much of biological motion can be understood as a coordinated system of periodic trajectories. For example, a point on the foot of a walker traces a periodic trajectory through space relative to the center of mass of the moving walker (Tsai et al., 1994). Furthermore, while the perception of biological motion certainly involves global processes (Chang & Troje, 2009a), local motions are shown to have unique and important information that is critical to distinguishing properties such as the direction that a point-light display is walking (Chang & Troje, 2009a). Sensitivity to curved trajectories has also been shown to underlie the ability to distinguish rigid from non-rigid motion (Todd, 1982), which is a highly relevant aspect of biological motion (Johansson, 1973). Similarly, observers are able to discriminate rigid from non-rigid motion based upon periodic deformations of a rotating object (Hogervorst, Kappers, & Koenderink, 1997; also see Braunstein, Hoffman, & Pollick, 1990; Domini, Caudek, & Proffitt, 1997; Todd & Norman, 1991). Second, they fit well with what we already know about the visual system's exquisite sensitivity to radial and circular patterns of form and motion (Beardsley & Vaina, 2005; Freeman & Harris, 1992; Loffler & Wilson, 2001; Morrone, Burr, & Vaina, 1995; Wilkinson, Wilson, & Habak, 1998). Third, they are amenable to a high degree of parametric control, allowing a broad and systematic testing of the visual system's response to this class of pattern.

Or et al. (2011) found that observers were able to detect amplitudes of 1–4 arcmin, and that local probability summation of the individual deformations along the trajectory could not account for this performance; rather, global pooling around the trajectory better accounted for the data. This evidence points to a locus of

☆ Parts of this work were previously reported at Vision Sciences Society. 12th Annual Meeting, May 11–16, 2012.

* Corresponding author.
E-mail addresses: marwan.daar@gmail.com (M. Daar), charles.or@psych.ucsb.edu (C.C.-F. Or), hrwilson@yorku.ca (H.R. Wilson).

0042-6989/$ - see front matter © 2012 Elsevier Ltd. All rights reserved.
http://dx.doi.org/10.1016/j.visres.2012.09.010

processing that can reliably detect deformations of circular motions. However, virtually nothing is known about this system's ability to discriminate varying degrees of deformation, which may underlie our ability to discriminate and identify variations in complex motions such as hand gestures and walking. As far as we know, only one other study touches upon this (Schill, Baier, & Stein, 2003). They found observers could discriminate, with an accuracy of about 75%, a trajectory whose curvature deviated by 8.4 arcmin relative to a reference trajectory of 4.8 arcmin. However, these trajectories were described by a simple open curve rather than a closed loop with multiple deformations, and within trials the directions of the two comparison trajectories were randomized relative to each other, presumably constraining performance to spatially invariant mechanisms. Perhaps more importantly, they did not have observers discriminate a curve from a straight line, and they only used one reference trajectory, so their data cannot be used to describe an incremental sensitivity to deformation of curved motion. Understanding how trajectory discrimination changes as a function of different reference trajectories may provide valuable insights into the underlying perceptual mechanisms. If, for example, the data are compatible with a response function with a threshold nonlinearity, this would suggest the presence of neural mechanisms tuned to deviations from circular motion trajectories, strengthening the findings from Or et al. On the other hand, a linear response function can be explained by an interaction of mechanisms that are not specialized for detecting such deviations. In order to test these possibilities, we systematically varied the amplitude of the trajectories, as this variable defines the degree to which the patterns deviate from a circular trajectory.

In the current study, we tested amplitude discrimination of RF trajectories relative to a number of different "pedestal" amplitudes. After replicating the detection condition from Or et al. (2011), we tested discrimination against reference trajectories whose amplitudes were set to 1X, 2.5X, 5X, 10X, and 15X the detection thresholds. We found that thresholds decreased dramatically at 1X and 2.5X, relative to detection, and then rose again as the pedestal amplitudes increased. We also show that this dipper shape generalizes to different radial frequencies, and different angular speeds. Finally, we provide a neural model that accounts for this pattern of data.

2. Methods

Our stimuli are described in detail in Or et al. (2011). Briefly, each motion trajectory comprises a dot whose polar location r at angular speed v and time t is:

$$r(vt) = r_o(1 + A\sin(\omega vt + \varphi)) \quad (1)$$

where r_o is the mean radius, A is the modulation amplitude, ω is the radial frequency (number of sinusoidal modulations per revolution), and φ is the phase (orientation of the trajectory). The polar angle $\theta = vt$. For our main experiment, we used a radial frequency of 3 cycles (RF3), and the mean radius was set to 1 degree of visual angle. The phase angle was always set to 90°, and the angular speed was 240°/s. The dot itself was a luminance profile defined by a radially symmetric difference of Gaussians (DOG):

$$\mathrm{DOG}(R) = 1.8\exp(-R^2/\sigma^2) - 0.8\exp(-R^2/(1.5\sigma)^2) \quad (2)$$

where R is the dot's radius. A value of 7.1 min of arc was chosen for σ, such that the peak spatial frequency would be 2.74 cpd and the bandwidth would be 1.79 octaves at half amplitude. The dot subtended about 0.75 degrees of visual angle across its width. The position of the dot was calculated over 168 frames, each lasting 9 ms, giving an impression of smooth motion. See Fig. 1. Stimuli

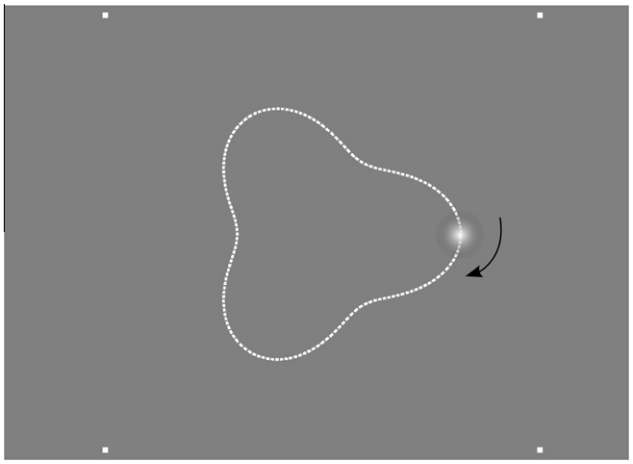

Fig. 1. Radial frequency motion trajectory for an RF3 pattern. The dotted line was not visible, and is shown here to illustrate the path that the dot takes. The four small squares depict the corners of an imaginary square that is used as a fixation reference: observers are asked to fixate at the approximate center of this square.

were presented on a CRT monitor with a refresh rate of 112 Hz, at a resolution of 800 × 600 pixels. At the viewing distance of 114 cm, the screen subtended 15.4° × 11.7°, with each square pixel subtending 1.18 min of arc. After gamma correction, the mean luminance of the display was 84 cd/m^2.

Observers were tested in a two-interval forced choice (2IFC) task using the method of constant stimuli (see Fig. 2). Following a 500 ms fixation, two successive RF trajectories separated by 1500 ms were binocularly presented. Observers were asked to indicate with a keypress which of the two trajectories had a higher amplitude. A second keypress initiated the subsequent trial. In each trial, one of the trajectories had an amplitude at a pedestal value, and the other one had one of five amplitude increments. Within each block, each increment was presented a total of 10 times, for a total of 50 trials per block. Observers ran four blocks for each condition. In the main experiment, there were a total of six conditions: Detection, 1X, 2.5X, 5X, 10X, and 15X. In the detection condition, the pedestal amplitude was set to 0 arcmin (a circle). After this condition was completed, the pedestal values in the remaining five conditions were determined as multiples of the detection threshold value. This was done on an individual basis, so for each condition, the pedestal amplitude varied between individuals. Block order for the non-detection conditions was counterbalanced across subjects. Throughout the trials, observers were asked to maintain fixation at the center of the screen (and therefore at the center of the trajectories). Instead of using a fixation cross, four corners of an imaginary square border were presented and subjects were asked to fixate at the approximate center of this border, whose length subtended 5 degrees of visual angle. This was done to ameliorate the issue of having a fixation cross act as a fixed reference point by which amplitude judgments could be aided (Whitaker & MacVeigh, 1990), especially with the larger amplitude conditions where the troughs of the radial modulations approached the center of the trajectory. More importantly, it removed a potential source of interference between the trajectory and a central fixation. Before each experimental session, practice trials with feedback were given, and amplitude increments were customized for each individual and condition. For each observer, data for each condition were pooled and fitted to a Quick (1974), or Weibull (1951) function using a maximum likelihood procedure to obtain the 75% amplitude discrimination thresholds. An example using sample data is shown in Fig. 3. Seven observers (2 females, mean age 28.14, SD = 4.41) participated in the main experiment for the first four

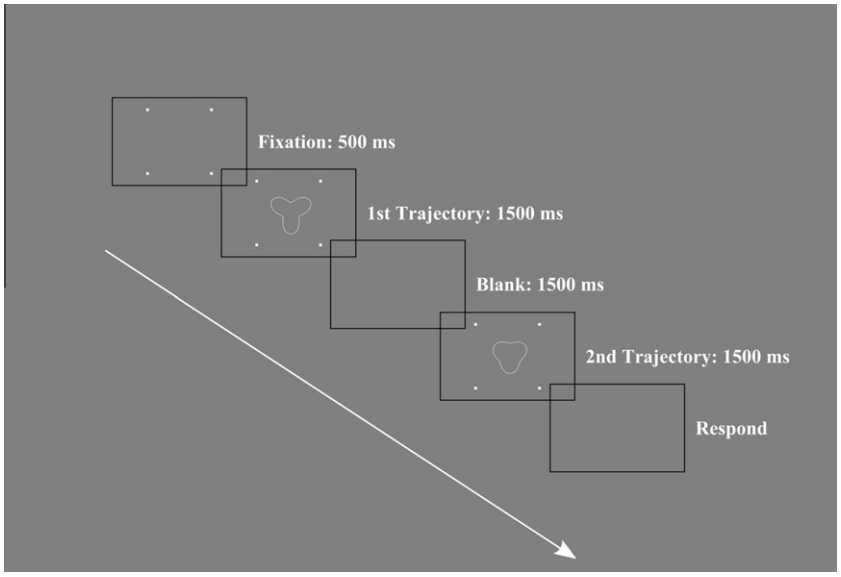

Fig. 2. Trial sequence: Following a 500 ms fixation, two RF trajectories are shown in succession, separated by a blank screen for 1500 ms. Observers then respond with a keypress to indicate which trajectory had a larger amplitude. In this example, the first trajectory is the correct response.

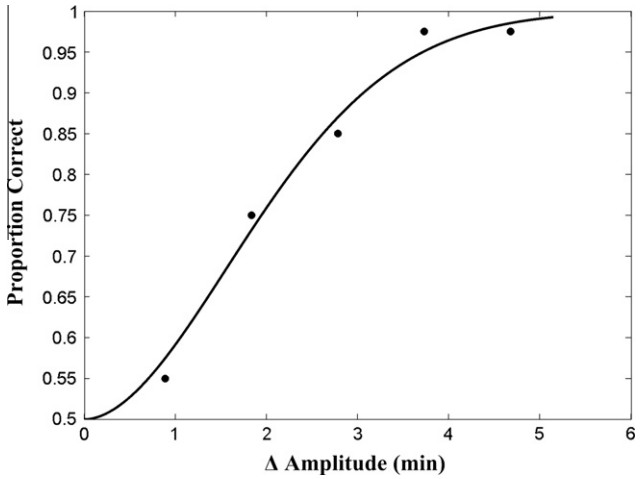

Fig. 3. Sample data showing a psychometric curve for one of the observers (AL). This example shows the pooled data for the detection condition. ΔAmplitude indicates the difference in amplitude between the pedestal amplitude and the increment amplitude. The data are fit to a Quick function using a maximum likelihood procedure, and 75% discrimination thresholds are reported.

conditions (detection, 1X, 2.5X, and 5X). Due to availability, only five observers ran for all six conditions (including 10X and 15X). All had normal or corrected to normal vision.

3. Results

In our main experiment, we measured amplitude detection thresholds across a number of different pedestal amplitudes. This was done to investigate how sensitivity to these patterns changes as a function of amplitude increment. Typical individual data for two observers are shown in Fig. 4, and the means across all observers are shown in Fig. 5. Relative to detection thresholds, increment thresholds dipped almost two fold at 2.5X, and then rose as the pedestal values increased, showing a classic dipper shape. Mean thresholds for detection, 1X, 2.5X, 5X, 10X, and 15X were 2.36, 1.26, 1.15, 1.95, 2.45, and 3.24 arcmin, respectively. A repeated measures ANOVA run across all seven subjects for the first four conditions showed a main effect of pedestal amplitude, $F(3,18) = 9.366$, $p < 0.001$. Sidak corrected pairwise comparisons showed a statistically significant difference between detection and the 2.5X ($p = 0.035$) conditions, and no difference between detection and 5X ($p = 0.741$). Detection vs. 1X showed a trend approaching significance ($p = 0.078$). A paired sample *t*-test run across the five subjects who completed the extra two conditions showed a significant difference between the 5X and 15X conditions ($p = 0.04$).

The above results are for RF3 trajectories at an angular speed of 240°/s. To determine whether this dipper generalized to other radial frequencies and speeds, two additional experiments were conducted. In the first of these, two observers, both of whom had participated in the main experiment, were tested with RF5 trajectories at an angular speed of 240°/s. The procedure was identical to the main experiment. As both observers in this experiment had shown more pronounced dips at the 1X compared to the 2X condition in the main experiment, they were tested only at detection, 1X, and 5X. The results are displayed in Fig. 6. For both observers, a clear dipper shape emerged.

In the next experiment, we investigated whether the pattern of thresholds seen thus far would be present at a faster angular speed. If so, this would strengthen the idea that the dipper shape reflects processing of the *shape* of the trajectory rather than being an artifact of sensitivity to a particular speed of motion. Two observers were tested with RF3 trajectories at an angular speed of 480°/s. As in the previous experiment, only detection, 1X, and 5X conditions were tested. The results are shown in Fig. 7, again revealing a dipper shape. Thus, the presence of dipper functions generalizes across both radial frequency and speed.

As a final control we tested to see whether this pattern of results could possibly reflect processing of static patterns induced by motion streaks (Geisler, 1999). Given the relatively high speed of these RF motion trajectories, it is conceivable that rather than discriminating motion patterns, observers were in fact discriminating RF patterns that were cortically represented as static RF patterns, which have been shown to produce dipper functions (Bell et al., 2009). To minimize any motion streaks, we reduced the contrast of the trajectory to 5%, as this manipulation has previously been shown to essentially eliminate motion streaks (Edwards & Crane, 2007). Two observers were tested with 5% contrast RF3

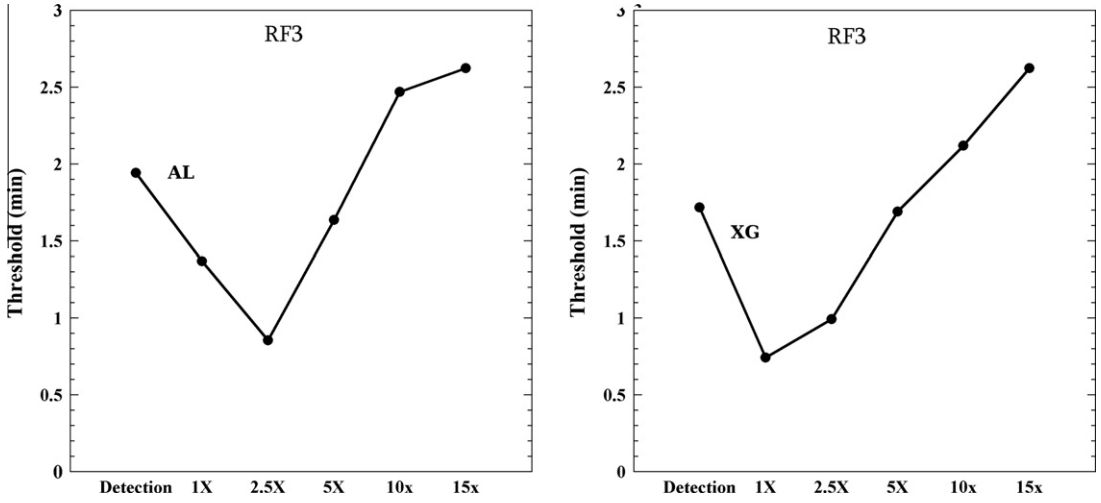

Fig. 4. Individual data from two observers for RF3 trajectories.

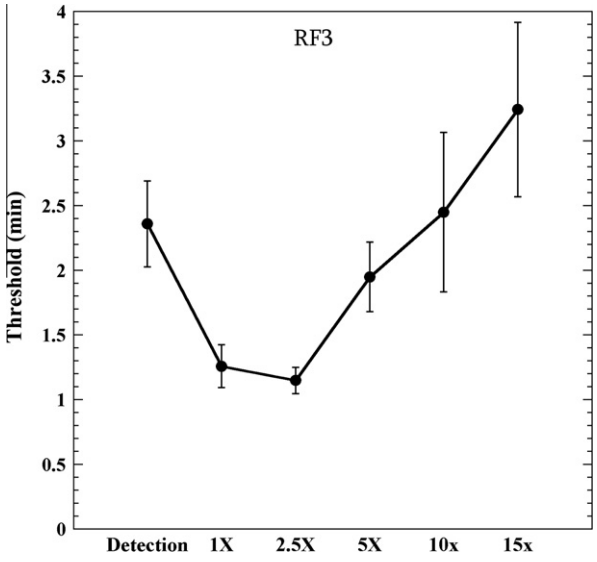

Fig. 5. Mean data across all subjects for our main experiment. The means and error bars for the first four conditions (detection – 5X) reflect data from all seven observers, while those for the last two conditions (10X, 15X) reflect data from five observers. Thresholds are in arcmin. Error bars indicate SEM.

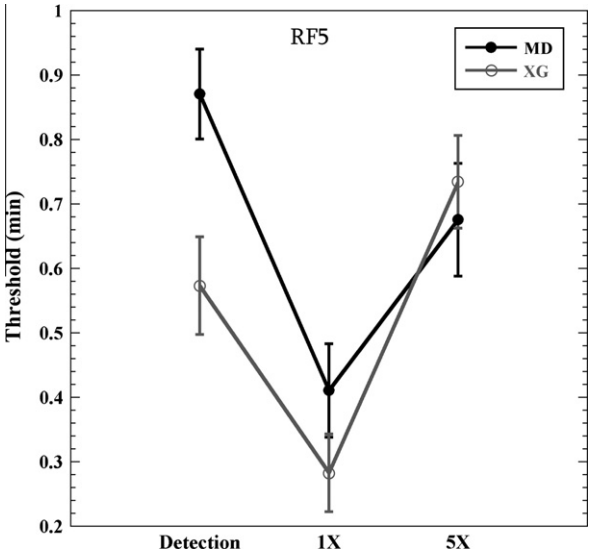

Fig. 6. Results for two observers tested with RF5 trajectories. Angular speed was the same as in the main experiment (240°/s). Error bars indicate bootstrapped standard deviations.

trajectories at an angular speed of 240°/s, at detection, 1X, and 5X. The results (Fig. 8) show a dipper, indicating that our results are due to curved motion per se rather than to motion streaks.

4. Discussion

The detection condition in our data successfully replicates Or et al. (2011), but more importantly a clear dipper shape emerges as a function of pedestal amplitude. This was reliable across all subjects, and generalized across radial frequency, angular speed, and contrast of the trajectory. When viewed across all subjects, thresholds were lowest in the 2.5X condition and rose back to detection levels by 5X. Interestingly, Bell et al. (2009) found a dipper shape for static RF patterns, where the thresholds also rose to detection levels at the 5X condition, and cited it as evidence of an independent channel for each static RF pattern. A plausible explanation for this dipper shape in our study is a population of cells that exhibit a non-linear response function for motion curvature (Nachmias & Sansbury, 1974; see Fig. 9). Such a mechanism could comprise units that, as a population, exhibit cumulative tuning to the amount of deviation from circular motion trajectories. The portion of the function below the threshold nonlinearity would reflect the fact that the units require a minimum level of input before they start to fire; the subsequent rise would reflect the approximately linear relationship between the increment threshold and the pedestal amplitude (Weber, 1834; Masin, Zudini, & Antonelli, 2009).

To explore this further, we modeled our data using a transducer function that has been found to be successful in modeling increment thresholds in other psychophysical domains such as contrast discrimination (see Wilson and Wilkinson (2002) for a review). The neural response (R) can be expressed as:

$$R = Mx^{N+\varepsilon}/(\sigma^N + x^N) \quad (3)$$

where x is the amplitude of the trajectory, M acts as a scaling constant, σ is a semi-saturation constant, and N is the steepness of the function. ε is a parameter that determines the rate of increase at large values of x. Note that when ε is set to 0, this is a Naka–Rushton function (Naka & Rushton, 1966).

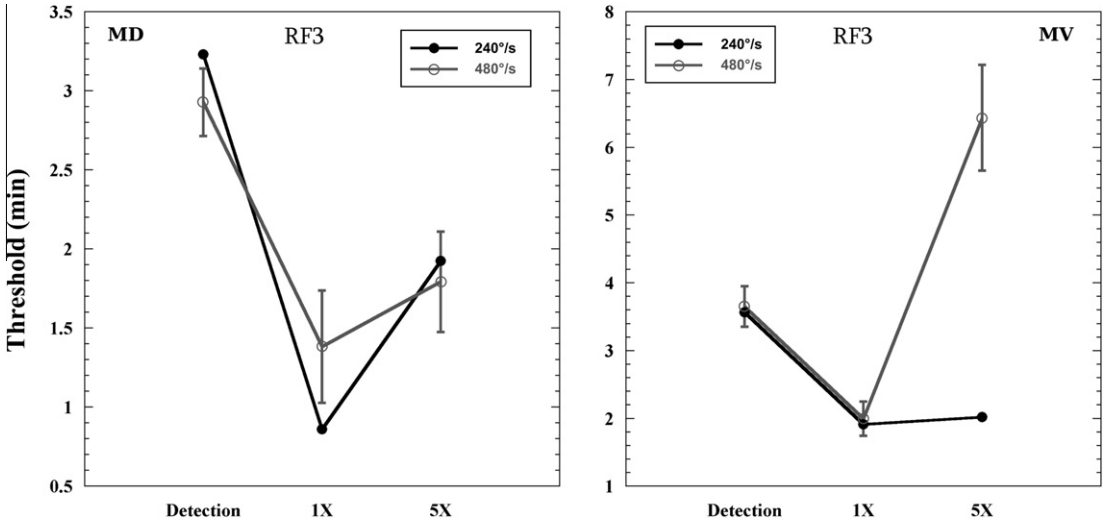

Fig. 7. Results for two observers tested at an angular speed of 480°/s with RF3 trajectories. The data from the main experiment (RF3, 240°/s) are also shown for comparison. Error bars indicate bootstrapped standard deviations.

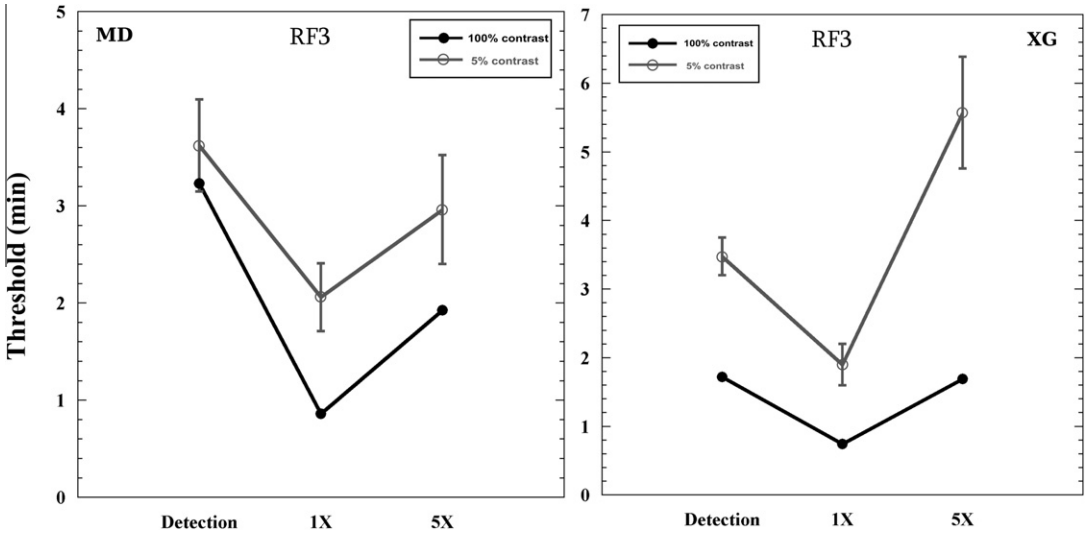

Fig. 8. Results for two observers tested at 5% contrast with RF3 trajectories at an angular speed of 240°/s. The data from the main experiment (RF3, 240°/s) are also shown for comparison. Error bars indicate bootstrapped standard deviations.

Model fitting was done by assuming that the neural response difference between each pedestal and its corresponding increment threshold remains constant across the different pedestal values. Setting this neural response difference at a constant of 1 unit, we used a least squares estimator to fit our obtained thresholds. The parameters that best fit our data are:

$m = 2.25$,
$\sigma = 4.35$,
$N = 1.67$,
$\varepsilon = 0.59$.

The model including predicted thresholds is shown in Fig. 10, and successfully accounts for two key features in our data. Both the dip and subsequent rise in thresholds are explained by the accelerating and compressive non-linearities respectively. Importantly, the evidence of a nonlinear transducer function suggests a set of specialized units that are sensitive to deviations from circular motion trajectories.

Our results shed light upon the response characteristics of the cells tuned to these trajectories, and allow us to speculate about a neurophysiological locus. The finding that the thresholds did not appreciably change over different speeds is consistent with many previous findings (de la Malla & López-Moliner, 2010; Nakayama & Tyler, 1981; Or et al., 2011), and suggests that discrimination of these trajectories may have more to do with the perception of shape rather than of motion per se. FMRI data from our laboratory (Gorbet, Wilkinson, & Wilson, 2011) are consistent with this idea, showing that this class of stimuli elicit a large BOLD response in V1 through V4, relative to linear sinusoidal trajectories. In addition, multivoxel pattern analysis shows that spatial patterns of activity in V2 and V3 successfully predict the radial frequency of the trajectories from RF2 through RF5. While the classifier averaged across RF amplitude, it is likely that these same cells represent amplitude information. Further fMRI experiments could test this possibility. Changes associated with variations in RF amplitude are relevant to the geometric variations associated with head outline viewpoint (Wilson et al., 2000) and identity (Wilson, Loffler, &

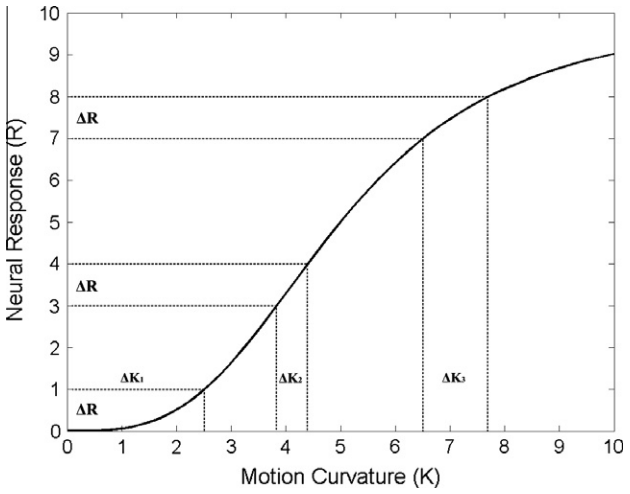

Fig. 9. Schematic representation of how a transducer function accounts for a dipper shape. ΔR indicates the minimal neural response that is required for discrimination. ΔK represents the corresponding just noticeable difference (JND). As the function is non-linear, the JNDs change depending on where along the function the discrimination is occuring. The smallest JNDs occur when the slope is the steepest (ΔK_2), and this corresponds to a dip in the increment thresholds. The units shown here are arbitrary.

Wilkinson, 2002), the latter of which is known to be processed in higher visual areas (Pourtois et al., 2005). Furthermore, static radial frequency patterns, which are well represented in V4 (Wilkinson et al., 2000), show a very similar dipper shape as a function of pedestal amplitude (Bell et al., 2009). However, the finding that the dipper function emerged even at a low contrast is powerful evidence that the mechanism underlying the perception of RF motion trajectories is quite distinct from that which processes static RF patterns.

The data from our RF5 stimuli show that sensitivity to motion trajectory amplitudes can approach a resolution of about 15 arcsec, which falls within the hyperacuity range (Westheimer, 1987). While this resolution is not as fine as that found in the detection of static radial frequency patterns (Wilkinson, Wilson, & Habak, 1998), it is still impressive considering the trajectory has to be integrated over a period of time. Other psychophysical studies have shown motion amplitude thresholds as low as 5–20 arcsec (de la Malla & López-Moliner, 2010; Nakayama & Tyler, 1981), although these used stimuli that comprised sinusoidally oscillating lines, where there are many local points that can be simultaneously integrated over space. Similarly, in a control experiment where observers had to detect periodic deformations of a object rotating along only one axis (Hogervorst, Kappers, & Koenderink, 1997), amplitude thresholds were too low to be measured given the resolution limitations of the display.

In most of our experimental conditions, the amplitudes of the RF trajectories were well above detection thresholds, making them suitable for understanding biological motion, which often involves trajectories that are far from circular (Chang & Troje, 2009b). However, as of yet it is unclear what role amplitude discrimination plays in the perception of biological motion. For example, one of the interesting findings from the biological motion literature is that observers are able to utilize the information in these periodic motion trajectories even with exposure times much shorter than the period of the motion. Chang and Troje (2008) found that performance in discriminating rightward vs. leftward point-light walkers did not deteriorate as a function of exposure time, even when this meant that only a fifth of the gait cycle was shown. In their other study (Chang & Troje, 2009b), even a tenth of the cycle contained enough information for observers to discriminate walking direction. However, performance in these tasks is based upon information contained in the direction of the trajectory, which is clearly discernible from partial trajectories (Chang & Troje, 2009b), rather than on subtle characteristics of its shape, such as amplitude. Nevertheless, it is certainly plausible that amplitude plays a crucial role in other contexts. An example may be interpreting the shape that the endpoint of a conductor's baton traces through space, where the amount of curvature carries important emotional information that is used by the musicians (Luck, Toiviainen, & Thompson, 2010).

5. Conclusions

In summary, we have found that amplitude discrimination of radial frequency trajectories shows a dipper shaped function as the amplitude of the reference trajectory is increased. Furthermore, this pattern is seen across different speeds, radial frequencies, and contrasts. Our model shows how a non-linear transducer function can account for these results, and provides insight into the mechanisms underlying the perception of periodic motion trajectories.

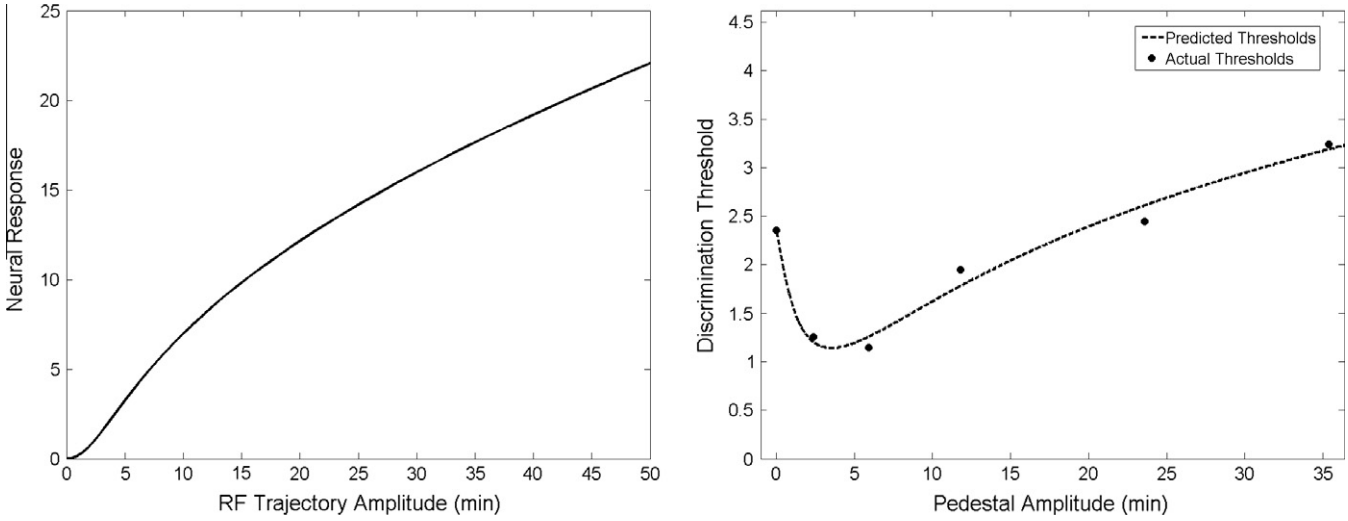

Fig. 10. On the left is shown our modeled transducer function. The slope of the function starts off shallow, quickly steepens, and then begins to flatten. On the right are shown the predicted thresholds based on the transducer function. Actual thresholds from our main experiment are also plotted.

Finally, this study further consolidates the viability of RF motion trajectories as a valuable tool in the study of motion perception.

References

Beardsley, S. A., & Vaina, L. M. (2005). Psychophysical evidence for a radial motion bias in complex motion discrimination. *Vision Research, 45*, 1569–1586.

Bell, J., Wilkinson, F., Wilson, H. R., Loffler, G., & Badcock, D. R. (2009). Radial frequency adaptation reveals interacting contour shape channels. *Vision Research, 49*, 2306–2317.

Braunstein, M. L., Hoffman, D. D., & Pollick, E. E. (1990). Discriminating rigid from nonrigid motion: Minimum points and views. *Perception and Psychophysics, 47*, 205–214.

Burr, D., & Thompson, P. (2011). Motion psychophysics: 1985–2010. *Vision Research, 51*, 1431–1456.

Chang, D. H. F., & Troje, N. F. (2008). Perception of animacy and direction from local biological motion signals. *Journal of Vision, 8*, 1–10 (article no. 3).

Chang, D. H. F., & Troje, N. F. (2009a). Characterizing global and local mechanisms in biological motion perception. *Journal of Vision, 9*, 1–10 (article no. 8).

Chang, D. H. F., & Troje, N. F. (2009b). Acceleration carries the local inversion effect in biological motion perception. *Journal of Vision, 9*, 1–17 (article no. 19).

de la Malla, C., & López-Moliner, J. (2010). Detection of radial motion depends on spatial displacement. *Vision Research, 50*, 1035–1040.

Domini, F., Caudek, C., & Proffitt, D. R. (1997). Misperceptions of angular velocities influence the perception of rigidity in the kinetic depth effect. *Journal of Experimental Psychology: Human Perception and Performance, 23*, 1111–1129.

Edwards, M., & Crane, M. F. (2007). Motion streaks improve motion detection. *Vision Research, 47*, 828–833.

Freeman, T. C., & Harris, M. G. (1992). Human sensitivity to expanding and rotating motion: Effects of complementary masking and directional structure. *Vision Research, 32*(1), 81–87.

Geisler, W. S. (1999). Motion streaks provide a spatial code for motion direction. *Nature, 400*, 65–69.

Gorbet, D. J., Wilkinson, F., & Wilson, H. R. (2011). An fMRI examination of the neural processing of periodic motion trajectories by the human visual system. Abstract 695.04, *Society for neuroscience annual meeting*.

Hogervorst, M. A., Kappers, A. M., & Koenderink, J. J. (1997). Monocular discrimination of rigidly and nonrigidly moving objects. *Perception and Psychophysics, 59*, 1266–1279.

Johansson, G. (1973). Visual perception of biological motion and a model for its analysis. *Perception and Psychophysics, 14*, 201–211.

Loffler, G., & Wilson, H. R. (2001). Detecting shape deformation of moving patterns. *Vision Research, 41*, 991–1006.

Luck, G., Toiviainen, P., & Thompson, M. R. (2010). Perception of expression in conductors' gestures: A continuous response study. *Music Perception, 28*, 47–57.

Masin, S. C., Zudini, V., & Antonelli, M. (2009). Early alternative derivations of Fechner's law. *Journal of the History of the Behavioral Sciences, 45*, 56–65.

Morrone, M. C., Burr, D. C., & Vaina, L. M. (1995). Two stages of visual processing for radial and circular motion. *Nature, 376*, 507–509.

Nachmias, J., & Sansbury, R. V. (1974). Letter: Grating contrast: Discrimination may be better than detection. *Vision Research, 14*, 1039–1042.

Naka, K. I., & Rushton, W. A. (1966). S-potentials from luminosity units in the retina of fish (Cyprinidae). *The Journal of Physiology, 185*, 587–599.

Nakayama, K., & Tyler, C. W. (1981). Psychophysical isolation of movement sensitivity by removal of familiar position cues. *Vision Research, 21*, 427–433.

Nishida, S. (2011). Advancement of motion psychophysics: Review 2001–2010. *Journal of Vision, 11*, 11.

Or, C. C.-F., Thabet, M., Wilkinson, F., & Wilson, H. R. (2011). Discrimination and identification of periodic motion trajectories. *Journal of Vision, 11*, 1–11.

Pourtois, G., Schwartz, S., Seghier, M. L., Lazeyras, F., & Vuilleumier, P. (2005). Portraits or people? Distinct representations of face identity in the human visual cortex. *Journal of Cognitive Neuroscience, 17*, 1043–1057.

Quick, R. F. (1974). A vector-magnitude model of contrast detection. *Kybernetik, 16*, 65–67.

Schill, K., Baier, V., & Stein, K. (2003). Motion shapes: Empirical studies and neural modeling. *Spatial Cognition III*, 305–320.

Todd, J. T. (1982). Visual information about rigid and nonrigid motion: A geometric analysis. *Journal of Experimental Psychology: Human Perception and Performance, 8*, 238–252.

Todd, J. T., & Norman, J. F. (1991). The visual perception of smoothly curved surfaces from minimal apparent motion sequences. *Perception and Psychophysics, 50*, 509–523.

Tsai, P.-S., Shah, M., Keiter, K., & Kasparis, T. (1994). Cyclic motion detection for motion based recognition. *Pattern Recognition, 27*, 1591–1603.

Weber, E. H. (1834). *De pulsu, resorptione, auditu et tactu. Annotationes anatomicae et physiologicae*. Leipzig: Koehler (cited in Masin, Zudini, & Antonelli, 2009).

Weibull, W. (1951). A statistical distribution function of wide applicability. *Journal of Applied Mechanics, 18*, 293–297.

Westheimer, G. (1987). Visual acuity and hyperacuity: Resolution, localization, form. *American Journal of Optometry and Physiological Optics, 64*, 567–574.

Whitaker, D., & MacVeigh, D. (1990). Displacement thresholds for various types of movement: Effect of spatial and temporal reference proximity. *Vision Research, 30*, 1499–1506.

Wilkinson, F., James, T. W., Wilson, H. R., Gati, J. S., Menon, R. S., & Goodale, M. A. (2000). An fMRI study of the selective activation of human extrastriate form vision areas by radial and concentric gratings. *Current Biology: CB, 10*, 1455–1458.

Wilkinson, F., Wilson, H. R., & Habak, C. (1998). Detection and recognition of radial frequency patterns. *Vision Research, 38*, 3555–3568.

Wilson, Hugh. R., Loffler, G., & Wilkinson, F. (2002). Synthetic faces, face cubes, and the geometry of face space. *Vision Research, 42*, 2909–2923.

Wilson, H. R., & Wilkinson, F. (2002). Spatial channels in vision and spatial pooling. In L. M. Chalupa & J. S. Werner (Eds.), *The visual neurosciences*. Cambridge, MA: MIT Press.

Wilson, H. R., Wilkinson, F., Lin, L. M., & Castillo, M. (2000). Perception of head orientation. *Vision Research, 40*, 459–472.